Molecular Crystals and Liquid Crystals
Publication details, including instructions for authors and subscription information:
http://www.tandfonline.com/loi/gmcl20

Influence of $TiCl_4$ Post-Treatment on TiO_2 Nanotube Arrays for Dye-Sensitized Solar Cells

Jeong-Hyun Park [a], Jae-Hong Kim [a], Chel-Jong Choi [b], Hyunsoo Kim [b] & Kwang-Soon Ahn [a]

[a] School of Chemical Engineering, Yeungnam University, Gyeongsan, 712-749, S. Korea

[b] School of Semiconductor and Chemical Engineering, Semiconductor Physics Research Center, Chonbuk National University, Jeonju, 561-756, S. Korea

Version of record first published: 17 Sep 2012.

To cite this article: Jeong-Hyun Park , Jae-Hong Kim , Chel-Jong Choi , Hyunsoo Kim & Kwang-Soon Ahn (2012): Influence of $TiCl_4$ Post-Treatment on TiO_2 Nanotube Arrays for Dye-Sensitized Solar Cells, Molecular Crystals and Liquid Crystals, 567:1, 19-27

To link to this article: http://dx.doi.org/10.1080/15421406.2012.702375

Mol. Cryst. Liq. Cryst., Vol. 567: pp. 19–27, 2012

ISSN: 1542-1406 print/1563-5287 online
DOI: 10.1080/15421406.2012.702375

Taylor & Francis
Taylor & Francis Group

Influence of $TiCl_4$ Post-Treatment on TiO_2 Nanotube Arrays for Dye-Sensitized Solar Cells

JEONG-HYUN PARK,[1] JAE-HONG KIM,[1] CHEL-JONG CHOI,[2] HYUNSOO KIM,[2,*] AND KWANG-SOON AHN[1,*]

[1]School of Chemical Engineering, Yeungnam University, Gyeongsan 712-749, S. Korea
[2]School of Semiconductor and Chemical Engineering, Semiconductor Physics Research Center, Chonbuk National University, Jeonju 561-756, S. Korea

Two types of TiO_2 nanotubes, conventional TiO_2 nanotube (Type I) and nanoporous layer-covered TiO_2 nanotube (Type II), were synthesized by electrochemical anodization for dye-sensitized solar cells (DSSCs). Those surfaces were treated with various concentrations of aqueous $TiCl_4$ (5-50 mM). DSSCs with the $TiCl_4$-treated Types I and II exhibited the optimized efficiencies in the 20 and 5 mM $TiCl_4$ treatments for the Types I and II nanotubes, respectively. The DSSC with 5 mM $TiCl_4$-treated type II exhibited much higher cell performance (5.5%) than that (4.1%) with 20 mM $TiCl_4$-treated Type I, indicating that the Type II nanotubes is more effective for the $TiCl_4$ surface treatment. The $TiCl_4$ treatment on the Type II nanotubes having fewer surface defect states led to significantly enhanced electron lifetime and electron transport, in addition to slightly increased amount of the adsorbed dyes, resulting in significantly improved cell efficiency. As the $TiCl_4$ concentration is further increased over the optimized concentration, the cell performances were gradually reduced for both of the Types I and II, due to the blocked voids and narrowed pores which facilitated the recombination reaction and shortened electron lifetime.

Keywords TiO_2 nanotube; surface treatment; dye-sensitized solar cell; electron lifetime; electron transport

1. Introduction

TiO_2-based dye-sensitized solar cells (DSSCs) have attracted large attention, due to their potential to become low-cost alternatives to commercial Si-based solar cells[1–3]. They consist of a dye-sensitized TiO_2 layer, a Pt counter electrode, and an electrolyte containing a redox couple (I^-/I_3^-) between the two. Dye molecules adsorbed on the TiO_2 can be excited by absorbing light. Photo-excited electrons of the dye molecules can then be injected into the conduction band of the TiO_2 and transferred to the transparent conducting oxide (TCO) for use in an external circuit.

Both of Prof. K. –S. Ahn and H. S. Kim contributed equally to this work as the corresponding authors.

*Address corresspondence to Prof. H. S. Kim. E-mail: hskim7@chonbuk.ac.kr

*Address corresspondence to Prof. K. –S. Ahn Tel: + 82-53-810-2524 Fax: +82-53-810-4631. E-mail: kstheory@ynu.ac.kr

Their performance has been improved by controlling the surface morphology and particle size of the TiO_2 layers [4, 5], and by developing new dyes [6] and electrolytes [7]. Conventional mesoporous TiO_2 films comprising nanoparticles smaller than 30 nm do not develop depletion layers at the interface with the electrolyte. When a bulk semiconductor is in contact with an electrolyte, a space charge region (depletion layer) is formed at the surface of the semiconductor to equalize the Fermi levels. The electric field formed in the depletion layer facilitates the separation of the photogenerated electrons and holes. However, unlike the bulk particles, the nanoparticles hardly form the depletion layer, which causes large back electron transfer from the conduction band of the TiO_2 to the electrolyte [8, 9]. Suppression of back electron transfer has been attempted by employing 1-dimensional nanostructures (nanotubes, nanorods, *etc.*) because they provide faster electron transport kinetics [5,10–12]. However, nanostructured DSSCs employing the nanotube arrays have not exhibited efficiencies as high as those with nanoparticles, mainly because of reduced dye adsorption by their lower surface areas [13, 14].

Post-treatment of mesoporous TiO_2 films with $TiCl_4$ has been widely used to increase the cell performance, because the $TiCl_4$ surface treatment has been known to increase surface area and improve electron transport, light scattering, purification of TiO_2, and anchoring of dyes [4, 12,13, 15–18]. However, although the $TiCl_4$ treatment may strongly depend on the initial TiO_2 materials, those effects have scarcely been studied [18].

In this article, the two types of TiO_2 nanotube arrays (Types I and II) were prepared on the Ti foils, where the former and latter are the conventional TiO_2 nanotube arrays (Type I) and nanoporous-layer-covered nanotube arrays (Type II). The $TiCl_4$ surface treatments were carried out for the Types I and II TiO_2 nanotubes by varying the $TiCl_4$ concentration from 5 to 50 mM. We found that the optimized $TiCl_4$ concentrations were 20 and 5 mM for the Types I and II, respectively, where the 5 mM $TiCl_4$–treated Type II provided much higher cell efficiency (5.5%) than the Type I (4.1%). It indicates that the Type II TiO_2 nanotube arrays are more effective for the $TiCl_4$ surface treatment, the detailed things of which were systematically studied in terms of morphologies of the TiO_2 nanotubes, electron transport, electron lifetime, recombination rate, and ion transport.

2. Experimental Details

2.1. Conventional TiO_2 nanotubes (1-step nanotubes, type I) grown on Ti foils

Ti foil (Goodfellow, 0.1 mm thickness, 99.6% purity) was used for the anodic growth of TiO_2 nanotubes. It was roughly ground, cleaned by sonication in acetone and ethanol and then rinsed with de-ionized water (DI). Electrochemical anodization was conducted at 60 V for 4 h with *ca.* 4 cm separation between the working (Ti foil) and the counter electrode (Pt mesh) in all cases. The electrolyte consisted of 0.25 wt.% NH_4F in ethylene glycol containing 1 M water. The 21 μm-thick, anodic TiO_2 nanotubes were sonicated in ethanol for 5 min to remove remnants from the surfaces and then dried in an air stream. They were then annealed at 450 °C for 4 h in air for improved crystallinity.

2.2. Nanoporous layer-covered TiO_2 nanotubes (2-step nanotubes, Type II) grown on Ti foils

Pretreated Ti substrates were prepared by the 1-step electrochemical formation of conventional TiO_2 nanotubes. Conventional TiO_2 nanotubes were then removed from the Ti

substrates by sonication in DI water for 5 min. A second anodization to form 21 μm-thick, nanoporous layer-covered TiO_2 nanotube arrays was performed under similar conditions to those of the 1-step TiO_2 nanotubes. The resulting 2-step TiO_2 nanotubes were sonicated in ethanol for 5 min to remove remnants from the surfaces and then dried in an air stream. They were annealed at 450 °C for 4 h in air to convert the amorphous phase to an anatase structure.

2.3. $TiCl_4$ post-treatment

Post-treatment with $TiCl_4$ has been carried out by the Types I and II TiO_2 nanotubes being soaked in $TiCl_4$ aqueous solutions with various $TiCl_4$ concentrations (5, 20, and 50 mM) for 30 min at 70 °C. After flushing with ethanol and drying, the electrodes were sintered again at 450 °C for 30 min.

2.4. Cell fabrication

Samples were dye-sensitized with Ru-based N3 dye [cis-bis (4,4′-dicarboxy-2, 2′-bipyridine) dithiocyanato ruthenium (II)] (Solaronix SA, Switzerland) by being immersed in dye solution at 40 °C for 24 h. Semitransparent Pt counter electrodes were prepared by doctor-blading Pt nanocluster-containing Pt paste (PT-1, Dyesol. Ltd.) onto F-doped SnO_2 (FTO) transparent conducting substrates and calcining at 450 °C for 30 min in air. The dye-adsorbed TiO_2 nanotube photoanodes and the semitransparent Pt counter electrodes were sandwiched with a liquid electrolyte containing the redox couple (I^-/I_3^-) introduced between them. All samples had similar active areas of dye-adsorbed photoanodes, 0.24 cm^2.

2.5. Characterization

The DSSCs were illuminated from the back-side, *i.e.*, from the semitransparent Pt counter electrode side, and their photovoltaic current-voltage characteristics were measured under 1 Sun illumination (100 $mWcm^{-2}$, AM 1.5) verified by an AIST-calibrated Si-solar cell. Nyquist and Bode plots were measured between 1 Hz and 100 kHz using an electrochemical impedance analyzer under 1 Sun at open-circuit potential. UV-Vis spectra were taken of dye molecules desorbed from the TiO_2 in 1 M aqueous NaOH. The TiO_2 nanotube arrays' morphologies were characterized by scanning electron microscopy (SEM, Hitachi FE-SEM S4800).

3. Results and Discussion

Figure 1 shows the top-viewed SEM images of the (a, b) untreated and (c, d) 50 mM $TiCl_4$-treated Types I and II TiO_2 nanotube arrays, respectively. The Type I arrays were composed of separated nanotubes of average diameter of 80±6 nm and average wall thickness of 9 nm. Each nanopore in the Type II corresponds to one nanotube (average diameter, 90 ± 10 nm; average wall thickness, 11 nm) and void areas on top were covered by nanoporous TiO_2 layers [19, 20], resulting in surface-interconnected nanopores (Figure 1 (b)). The Type I exhibited the bundling of the nanotubes, due to liquid-meniscus-induced capillary forces, which causes many defects (recombination centers) [19–21]. The capillary stress created during evaporative drying of liquids from the wetted TiO_2 nanotube arrays produce bundling and microcrack formation and the resulting morphological disorder gives rise to the distortion-induced surface defects mostly near the substrate which play a role as

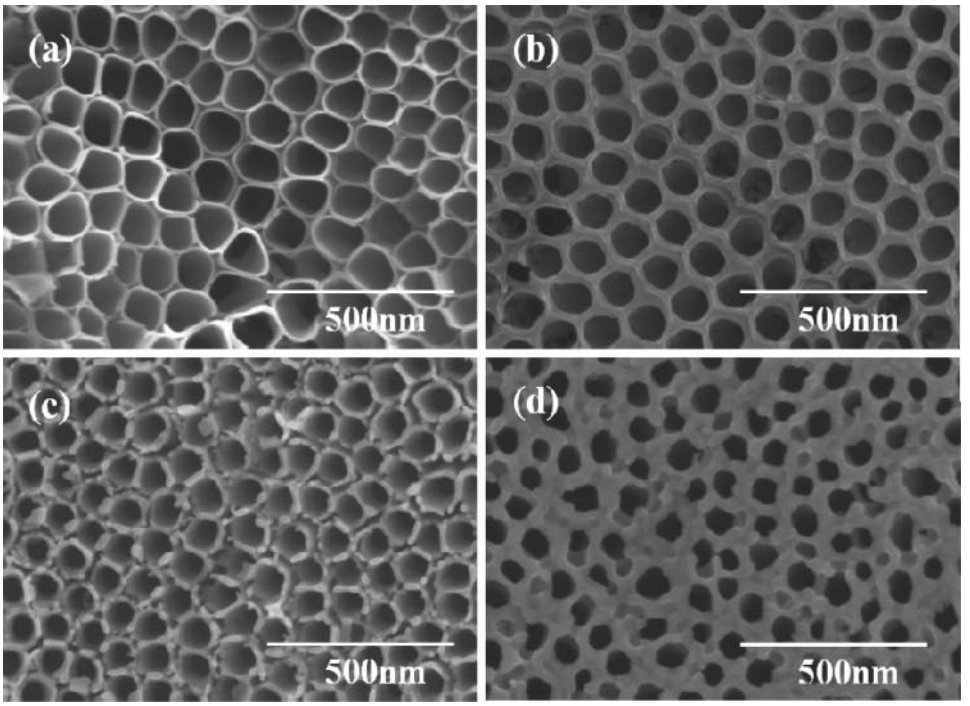

Figure 1. The top-viewed SEM images of the (a, b) untreated and (c, d) 50 mM $TiCl_4$-treated Types I and II TiO_2 nanotube arrays, respectively.

the surface recombination centers [21]. On the contrary, the Type II nanotube arrays have relatively fewer defects, because the surface-interconnected nanopores help to keep the nanotubes in a parallel arrangement and prevent them from bundling [19]. The difference in the morphologies of the TiO_2 nanotubes may have significant influence on the effects of the $TiCl_4$ post-treatment. The Types I and II nanotubes treated by 5 and 20 mM $TiCl_4$ exhibited no apparent morphological differences in the SEM images (not shown here), compared to the untreated samples, due to the low concentration of $TiCl_4$. However, treatment in the 50 mM $TiCl_4$ led to the excessive formation of TiO_2 on the nanotubes' surfaces, resulting in the blocked voids between the nanotubes for the Type I and the narrowed pores for the Type II, as seen in Figs. 1(c) and (d).

The amount of the adsorbed N3 dyes, measured by the UV-Vis spectroscopy, were estimated to be 4.4×10^{-7}, 5.2×10^{-7}, 5.8×10^{-7}, and 6.1×10^{-7} molcm^{-2} for the untreated, 5, 20, and 50 mM $TiCl_4$-treated Type I nanotubes, respectively. The untreated, 5, 20, and 50 mM $TiCl_4$-treated Type II nanotubes exhibited the amount of the adsorbed dyes of 3.5×10^{-7}, 4.3×10^{-7}, 5.2×10^{-7}, and 4.5×10^{-7} molcm^{-2}, respectively. The extent of the dye adsorption corresponds to the active surface areas of the TiO_2 that facilitate the anchoring of dye molecules [13, 15]. $TiCl_4$ surface treatment enhanced dye adsorption for both of Types I and II nanotubes, mainly due to the purification and passivation of the TiO_2 surface, leading to the increased active area [4, 12, 13, 15–18]. The Type I nanotubes exhibited higher amount of the adsorbed dyes than the Type II for each $TiCl_4$ concentration, indicating higher surface area. The 50 mM $TiCl_4$-treated Type II sample exhibited the lower amount of the adsorbed dyes than the 20 mM $TiCl_4$-treated Type II. The

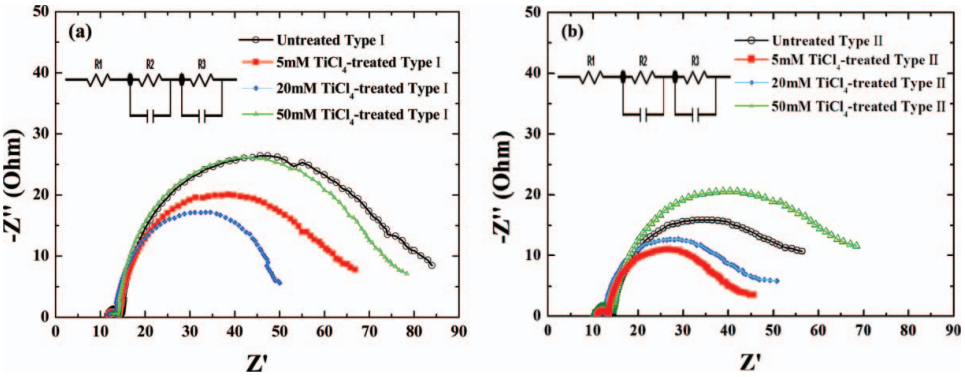

Figure 2. Nyquist plots of the DSSCs based on the (a) Type I and (b) Type II TiO_2 nanotubes, respectively, with and without the $TiCl_4$ surface treatment measured at open circuit voltage (V_{oc}) under 1 Sun illumination. (Color figure available online).

50 mM $TiCl_4$ treatment on the Type II exhibited the pores narrowed by the increased wall thickness (Fig. 1(d)). The active surface area of the TiO_2 affects the amount of the adsorbed dyes. The porosity of the nanotube array is decreased by the increased wall thickness and the decreased pore diameter. Therefore, the narrowed pores of the 50 mM $TiCl_4$-treated Type II decrease the porosity, leading to the reduced surface area and lower amount of the adsorbed dyes.

Figure 2 shows the Nyquist plots of the DSSCs based on the (a) Type I and (b) Type II TiO_2 nanotubes, respectively, with and without the $TiCl_4$ surface treatment measured at open circuit voltage (V_{oc}) under 1 Sun illumination. The semicircles at high- and low-frequencies arose from electrochemical reaction resistance at the Pt counter electrode (R2 in inset of Fig. 2) and charge transfer resistance at the TiO_2/dye/electrolyte interface (R3), respectively [15, 19]. The DSSC with the untreated Type II nanotubes exhibited lower R3 than that with the untreated Type I, indicating faster electron transport. It can be due to fewer surface defects (or recombination traps) in the well-aligned Type II nanotube arrays, where the surface defects are the Ti^{3+} surface states originated from the terminated surface of the TiO_2. The DSSCs with Type II nanotubes treated by 5 and 20 mM $TiCl_4$ exhibited much lower R3 values than those with the corresponsive $TiCl_4$-treated Type I nanotubes, indicating much faster electron transport. That is, $TiCl_4$ surface treatment on the less defective morphology resulted in significantly improved electron transport. Further increased, 50 mM $TiCl_4$ treatment remarkably increased R3 values back for all of the Types I and II. It can be attributed to the excessive formation of the semiconducting TiO_2 on the voids and/or pores, which leads to the 3-dimensional electron pathways and retards the electron transport.

Figure 3 shows the Bode plots of the DSSCs based on the (a) Type I and (b) Type II TiO_2 nanotubes, respectively, with and without the $TiCl_4$ surface treatment measured at open circuit voltage (V_{oc}) under 1 Sun illumination. The middle-frequency region (1 – 100 Hz) relates directly to electron transfer process at the interface between TiO_2 and dye and electrolyte [6, 7]. Electron lifetime (τ_e) in the mesoporous films was estimated using the equation $\tau_e = 1/(2\pi f_{mid})$, where f_{mid} is the peak frequency in the middle-frequency region. The shift of the f_{mid} peak from high frequency to low frequency reveals longer electron lifetime. Electron lifetimes were estimated to be 43, 41, 47, and 43 ms for the untreated, 5, 20, and 50 mM $TiCl_4$-treated Type I nanotubes, respectively. The untreated, 5,

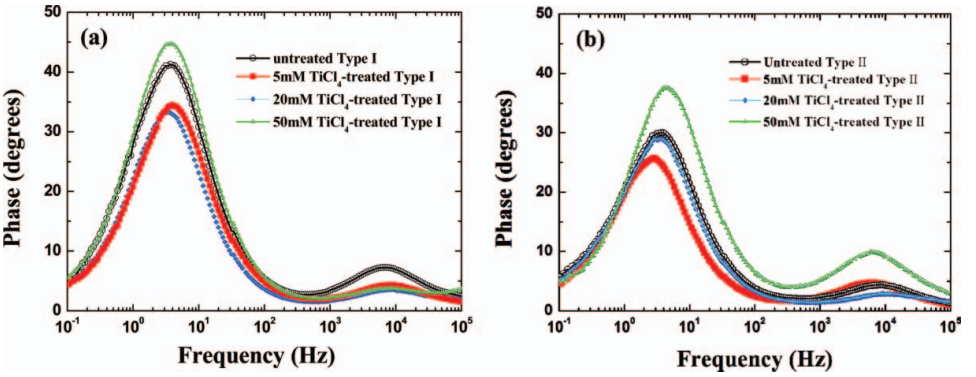

Figure 3. Bode plots of the DSSCs based on the (a) Type I and (b) Type II TiO_2 nanotubes, respectively, with and without the $TiCl_4$ surface treatment measured at open circuit voltage (V_{oc}) under 1 Sun illumination.

20, and 50 mM $TiCl_4$-treated Type II nanotubes exhibited the electron lifetimes of 41, 54, 47, and 37 ms, respectively. The electron lifetime on the Type I was slightly increased by 20 mM $TiCl_4$ concentration, whereas the Type II exhibited significantly enhanced electron lifetime only by 5 mM $TiCl_4$ surface treatment. It indicates that the $TiCl_4$ post-treatment on the TiO_2 morphology having fewer defects could significantly improve the electron lifetime. However, high $TiCl_4$ concentration (e.g. 50 mM) in the $TiCl_4$ treatment reduced the electron lifetime back. This can be because the excessive TiO_2 produced by high $TiCl_4$ concentration causes the 3-dimensional electron pathways, facilitating the recombination reaction of the electrons and the redox couple.

Figure 4 shows photovoltaic performances of the DSSCs based on the (a) Type I and (b) Type II TiO_2 nanotubes, respectively, with and without the $TiCl_4$ surface treatment measured under 1 Sun illumination, which are summarized in Table 1. The $TiCl_4$ surface treatment could improve overall energy conversion efficiency for the DSSCs with the Types I and II. As the $TiCl_4$ concentration increased to 20 mM, the cell efficiency of the DSSC based on the Type I nanotube arrays was improved to 4.1%. It can be due to the significantly

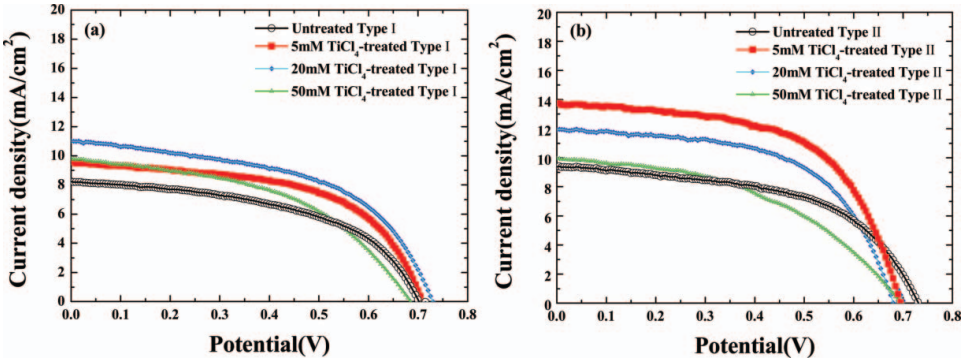

Figure 4. photovoltaic performances of the DSSCs based on the (a) Type I and (b) Type II TiO_2 nanotubes, respectively, with and without the $TiCl_4$ surface treatment measured under 1 Sun illumination.

Table 1. Photovoltaic performances of the DSSCs based on the Types I and II TiO_2 nanotube arrays with and without the $TiCl_4$ treatments.

Samples	$TiCl_4$ concentration	J_{sc} $mAcm^{-2}$	V_{oc} V	FF %	η %
Type I	Untreated	8.2	0.71	49.31	2.9
	5 mM	9.6	0.71	55.47	3.8
	20 mM	11.1	0.72	51.19	4.1
	50 mM	9.8	0.69	47.15	3.2
Type II	Untreated	9.3	0.72	53.54	3.7
	5 mM	13.7	0.70	58.04	5.5
	20 mM	11.9	0.70	55.87	4.7
	50 mM	10.0	0.71	44.23	3.1

increased amount of the adsorbed dyes and improved electron transport, as seen in Fig. 2. For the Type II, the DSSC with the only 5 mM $TiCl_4$-treated Type II nanotube arrays exhibited the optimized cell performance, whose efficiency (5.5%) was much higher than that (4.1%) of the DSSC with the optimized $TiCl_4$(20 mM)-treated Type I. The DSSC with the $TiCl_4$-treated Type I nanotubes optimized by 20 mM $TiCl_4$ resulted in the cell efficiency (4.1%) improved by 41% over that of the cell with the untreated Type I nanotubes (2.9%). The efficiency (5.5%) of the DSSC with the $TiCl_4$-treated Type II nanotubes optimized by 5 mM $TiCl_4$ was increased about 49% over that of the DSSC with untreated Type II nanotubes. It should be noted that the amount of the adsorbed dyes of the $TiCl_4$-treated Type I nanotubes optimized by 20 mM $TiCl_4$ was 5.8×10^{-7} $molcm^{-2}$ increased by 32% over that (4.4×10^{-7} $molcm^{-2}$) of the untreated Type I. In contrast, the $TiCl_4$-treated Type II nanotubes optimized by 5 mM $TiCl_4$ exhibited only 4.3×10^{-7} $molcm^{-2}$, which is only 22.8% increase over that (3.5×10^{-7} $molcm^{-2}$) of the untreated Type II. That is, although the $TiCl_4$-treated Type II nanotubes optimized by 5 mM $TiCl_4$ had less increased dye adsorption than $TiCl_4$-treated Type I nanotubes optimized by 20 mM $TiCl_4$, the 5 mM $TiCl_4$-treated Type II exhibited much more increased cell efficiency when fabricated in the DSSC. It indicates that the other dominant factors in addition to the increased dye adsorption contributed to the significantly enhanced cell efficiency of the DSSC with the optimized $TiCl_4$(5 mM)-treated Type II. The $TiCl_4$-treated Type II nanotubes exhibited much faster electron transport than the $TiCl_4$-treated Type I nanotubes (Fig. 2). Furthermore, the 5 mM $TiCl_4$-treated Type II exhibited significantly improved electron lifetime, as seen in Fig. 3. That is, the 5 mM $TiCl_4$ treatment on the Type II nanotubes led to the significantly enhanced electron lifetime and much faster electron transport, despite having less increased amount of the adsorbed dyes, which is responsible for the significantly enhanced cell efficiency (5.5%). The $TiCl_4$ treatment in the high $TiCl_4$ concentration (e.g. 50 mM) reduced the cell efficiencies for the both of the Types I and II by the decreased short-circuit current and, in particular, significantly lowered fill factors. The excessive TiO_2 formation on the nanotubes' surfaces led to not only the blocked voids and the narrowed pores for the Types I and II, respectively (Fig. 1) but also the 3-dimensional electron pathways. They resulted in the facilitated recombination reaction of the electrons and the redox couple and significantly reduced electron lifetime, as seen in Figs. 2 and 3, which are responsible for the much lower fill factors.

4. Conclusion

We prepared two types of TiO_2 nanotubes, conventional TiO_2 nanotube (Type I) and nanoporous layer-covered TiO_2 nanotube (Type II), as the starting materials for the $TiCl_4$ post-treatment. The Type I has many distortion-induced surface defects by the bundling during the drying procedure, whereas the Type II has fewer defects, owing to the surface-interconnected nanopores which prevent them from the bundling. Surfaces of the Types I and II were then post-treated by the $TiCl_4$ surface treatment with different concentrations of $TiCl_4$ (5, 20, and 50 mM). The cell efficiencies of the DSSCs with the $TiCl_4$-treated Types I and II were optimized by the 20 and 5 mM $TiCl_4$ treatments for the Types I and II, respectively. The 5 mM $TiCl_4$–treated Type II led to much higher cell efficiency (5.5%) than the 20 mM $TiCl_4$–treated Type I (4.1%), despite having less increased amount of the adsorbed dyes. We found that the 5 mM $TiCl_4$ treatment on the Type II nanotubes led to the significantly enhanced electron lifetime and much faster electron transport, which was responsible for the significantly enhanced cell efficiency (5.5%). The $TiCl_4$ treatments in the $TiCl_4$ concentration over the optimized concentration reduced the cell performances for both of the Types I and II. This can be attributed to the excessive TiO_2 formation on the surfaces which caused the blocked voids and the narrowed pores, leading to the facilitated recombination rate and poor electron lifetime. These results should provide good insights into surface treatment for the enhancement of nanostructured electrodes for the applications such as the DSSC, photoelectrochemical water-splitting cells, batteries, *etc*.

Acknowledgment

This research was supported by the Yeungnam University research grant and the Human Resources Development Program of Korea Institute of Energy Technology Evaluation and Planning (KETEP) grant (No. 20104010100580) funded by the Korean Ministry of Knowledge Economy.

References

[1] O'Regan, B., & Grätzel, M. (1991). *Nature*, *353*, 737.
[2] Lee, J. P., Yoo, B., Suresh, T., Kang, M. S., Vital, R., & Kim, K. J. (2009). *Electrochim. Acta*, *54*, 4365.
[3] Grätzel, M. (2001). *Nature*, *414*, 338.
[4] Mor, G. K., Shankar, K., Paulose, M., Varghese, O. K., & Grimes, C. A. (2006). *Nano Lett. 6*, 215.
[5] Nah, Y. C., Paramasivam, I., & Schmuki, P. (2010). *ChemPhysChem*, *11*, 2698.
[6] Yum, J. H., Jung, I., Baik, C., Ko, J. J., Nazeeruddin, M. K., & Grätzel, M. (2009). *Energy & Environ. Sci.*, *2*, 100.
[7] Kang, M. S., Ahn, K. S., Lee, J. W., & Kang, Y. S. (2008). *J. Photochem. & Photobiol. A: Chem.*, *195*, 198.
[8] Archer, M. D., Nozik, A. J., *et al.* (2008). Nanostructured and photoelectrochemical systems for solar photon conversion. R. J. D. Miller, R. Memming (Eds.), Chapter 2, p. 130, Imperial College Press: Singapore.
[9] Ahn, K. S., Kang, M. S., Lee, J. K., Shin, B. C., & Lee, J. W. (2006). *Appl. Phys. Lett.*, *89*, 013103.
[10] Nacak, J. M., Tsuchiya, H., Taveira, L., Aldabergerova, S., & Schmuki, P. (2005). *Angew. Chem. Int. Ed.*, *44*, 7463.
[11] Kang, S. H., Kim, Y. S., Kim, J. Y., & Sung, Y. E. (2009). *Nanotechnol. 20*, 355307.

[12] Paulose, M., Shankar, K., Varghese, O. K., Mor, G. K., & Grimes, C. A. (2006). *J. Phys. D: Appl. Phys. 39*, 2498.
[13] Charoensirithavorn, P., Ogomi, Y., Sagawa, T., Hayase, S., & Yoshikawa, S. (2010). *J. Electrochem. Soc. 157*, B354.
[14] Yip, C. T., Mak, C. S. K., Djurišić, A. B., Hsu, Y. F., & Chan, W. K. (2008). *Appl. Phys. A*, *92*, 589.
[15] An, S. Y., Park, J. H., Kim, J. H., Choi, C. J., Kim, H. S., & Ahn, K. S. J. (2011). *Nanosci. & Nanotech*. In press.
[16] Roy, P., Kim, D., Paramasivam, I., & Schmuki, P. (2009). *Electrochem. Commun. 11*, 1001.
[17] Fuke, N., Katoh, R., Islam, A., Kasuya, M., Furube, A., Fukui, A., Chiba, Y., Komiya, R., Yamanaka, R., Han, L., & Harima, H. (2009). *Energy & Environ. Sci. 2*, 1205.
[18] O'Regan, B. C., Durrant, J. R., Sommeling, P. M., & Bakker, N. J. (2007). *J. Phys. Chem. C*, *111*, 14001.
[19] Park, J. H., Kim, J. Y., Kim, J. H., Choi, C. J., Kim, H. S., Sung, Y. E., & Ahn, K. S. (2011). *J. Power Sources. 5*, 14569.
[20] Wang, D., Yu, B., Wang, C., Zhou, F., & Liu, W. (2009). *Adv. Mater. 21*, 1964.
[21] Chandra, D., & Yang, S. (2010). *Acc. Chem. Res. 43*, 1080.